Use of Poly(*o*-toluidine)/ZrO_2 Nanocomposite Coatings for the Corrosion Protection of Mild Steel

Sudeshna Chaudhari,[1] P. P. Patil,[1] A. B. Mandale,[2] K. R. Patil,[2] S. R. Sainkar[2]

[1]*Department of Physics, North Maharashtra University, Jalgaon 425 001, Maharashtra, India*
[2]*Center for Materials Characterization, National Chemical Laboratory, Pashan, Pune 411 008, Maharashtra, India*

Received 20 November 2006; accepted 24 January 2007
DOI 10.1002/app.26469
Published online 18 June 2007 in Wiley InterScience (www.interscience.wiley.com).

ABSTRACT: This study explored the possibility of using poly(*o*-toluidine) (POT)/ZrO_2 nanocomposite coatings for the corrosion protection of mild steel in a chloride environment. POT/ZrO_2 nanocomposite coatings were synthesized on steel substrates through an electrochemical route. These coatings were characterized with cyclic voltammetry, ultraviolet–visible absorption spectroscopy, Fourier transform infrared spectroscopy, scanning electron microscopy, and X-ray photoelectron spectroscopy. The performance of POT/ZrO_2 nanocomposites as protective coatings against the corrosion of mild steel in aqueous 3 wt % NaCl was evaluated with the potentiodynamic polarization technique and electrochemical impedance spectroscopy. The results of this study demonstrate that POT/ZrO_2 nanocomposite coatings provide better protection for mild steel against corrosion than pure POT coatings. The corrosion potential was about 0.312 V versus a saturated calomel electrode, more positive in aqueous 3 wt % NaCl for the nanocomposite-coated steel than the uncoated steel, and the corrosion rate of steel was reduced by a factor of almost 51. © 2007 Wiley Periodicals, Inc. J Appl Polym Sci 106: 220–229, 2007

Key words: coatings; conjugated polymers; FTIR; nanocomposites; synthesis

INTRODUCTION

During the last decade, electrically conducting polymers have been a center of scientific interest and active multidisciplinary research because of their excellent potential for widespread technological applications.[1–5] Several studies have been carried out recently or are in progress concerning the use of conducting polymer coatings for the corrosion protection of oxidizable metals.[6–9] Electrochemical polymerization is a simple, relatively inexpensive, and very convenient route for synthesizing novel conducting polymers on metallic surfaces. It has now become apparent that a careful choice of the solvent and/or supporting electrolyte and the establishment of electrochemical parameters are necessary for a successful electrochemical synthesis of conducting polymer coatings on oxidizable metals.[10,11]

Recently, considerable research interest has developed in synthesizing metal and/or metal oxide nanoparticle incorporated polymer matrices with interesting physical properties and tremendous application potential in diversified areas such as physics, chemistry, materials science, optics, microelectronics, and biomedical science.[12–18] Platinum,[12] palladium,[13] gold,[14] and copper[15] nanoparticles have been successfully incorporated into polyaniline and its substituted derivatives. The first attempt to electrochemically synthesize TiO_2- and WO_3-incorporated polypyrrole films on Au or indium tin oxide electrodes was made by Yoneyama and coworkers.[16,17] Ferreira et al.[18] showed that TiO_2 incorporation in the polypyrrole matrix during electrochemical synthesis on mild steel leads to the formation of polypyrrole/TiO_2 composite films. Furthermore, these composite films exhibit a slight improvement in the corrosion protection of mild steel in aqueous 3.5% NaCl solutions in comparison with pure polypyrrole.

In this work, we attempted to synthesize strongly adherent ZrO_2-nanoparticle-incorporated poly(*o*-toluidine) (POT) coatings on mild steel from an aqueous tartrate solution by using cyclic voltammetry. To the best of our knowledge, there are no reports in the literature dealing with the electrochemical synthesis of corrosion-protective ZrO_2-nanoparticle-incorporated POT coatings on mild steel from an aqueous tartrate medium. These coatings were characterized with cyclic voltammetry, ultraviolet–visible (UV–vis) absorption spectroscopy, Fourier transform infrared (FTIR) spectroscopy, scanning electron microscopy (SEM), and X-ray photoelectron spectroscopy (XPS). The ZrO_2 nanoparticles were successfully incorpo-

Correspondence to: P. P. Patil (pnmu@yahoo.co.in).
Contract grant sponsor: Defence Research and Development Organization (through the Defense Research and Development Organization (DRDO)/Indian Space Research Organization (ISRO)-PUNE University Interaction Cells, University of Pune, India).
Contract grant sponsor: University Grants Commission (New Delhi, India); contract grant number: F 30-14/2004(SR).

© 2007 Wiley Periodicals, Inc.
WILEY InterScience® DISCOVER SOMETHING GREAT

rated into the POT matrix and resulted in the formation of poly(*o*-toluidine)/ZrO_2 (POTZRO) nanocomposite coatings on mild steel. The corrosion protection performance of these coatings was examined in an aqueous 3 wt % NaCl solution by the use of the potentiodynamic polarization technique and electrochemical impedance spectroscopy (EIS). The results of this study demonstrate that the incorporation of ZrO_2 nanoparticles into the POT matrix reduces the corrosion rate (CR) of mild steel by a factor of almost 51.

EXPERIMENTAL

Analytical-reagent-grade chemicals were used throughout this study. The *o*-toluidine monomer was double-distilled before its use. In this work, an aqueous solution containing 0.1*M* sodium tartrate and 0.1*M* *o*-toluidine was used as the electrolyte, and it is called the standard electrolyte in the remaining text.

The chemical composition (wt %) of the mild steel used in this study was 0.03% C, 0.026% S, 0.01% P, 0.002% Si, 0.04% Ni, 0.002% Mo, 0.16% Mn, 0.093% Cu, and 99.64% Fe. The mild steel substrates ($\sim$ 10 mm $\times$ 15 mm $\times$ 0.5 mm) were polished with a series of emery papers of different grit sizes (180, 400, 600, 800, and 1200). After polishing, the substrates were cleaned with acetone and double-distilled water and dried in air. Before any experiment, the substrates were treated as described and freshly used with no further storage.

In a typical experiment, 40-nm ZrO_2 powder (1.25 g/L) was added to double-distilled water and sonicated for 1 h. Subsequently, in this emulsion solution, 0.1*M* sodium tartrate and 0.1*M* *o*-toluidine were dissolved with vigorous magnetic stirring for 30 min. The POTZRO nanocomposite coatings were synthesized by electrochemical polymerization in a ZrO_2-containing standard electrolyte with slow magnetic stirring through cyclic voltammetry.

The electrochemical polymerization experiments were carried out with the setup described in our previous article.[19] The synthesis of POTZRO coatings was performed by continuous cycling of the electrode potential between -0.5 and 1.8 V at a potential scan rate of 0.02 V/s. After deposition, the working electrode was removed from the electrolyte, rinsed with double-distilled water, and dried in air. For comparison, pure POT coatings were also synthesized under experimental conditions identical to those mentioned previously for the standard electrolyte without ZrO_2 powder.

The adhesion of the POT and POTZRO coatings was determined by the standard cellotape test (TESA 4204 BDF), which consists of cutting the coating into small squares, sticking the tape, and then stripping it. The percentage adherence was calculated from the ratio of the number of the remaining adherent coating squares to the total number of the squares.

The FTIR transmission spectra of the coatings were recorded in the spectral range of 4000–400 cm^{-1} with a PerkinElmer (Wellesley, MA) 1600 series II spectrometer. The optical absorption studies of these coatings were carried out *ex situ* at room temperature in the wavelength range of 300–1100 nm with a Hitachi model U2000 microprocessor-controlled, double-beam UV–vis spectrophotometer. SEM was employed to characterize the surface morphology with a Leica (Cambridge, UK) Cambridge 440 microscope. The XPS analysis was carried out with a V.G. Microtech Scientific (Crawley, UK) ESCA 3000 spectrometer equipped with two ultrahigh-vacuum chambers. The pressure in the chambers during the experiments was about 10^{-9} Pa. The XPS spectra were recorded with unmonochromatized Mg Kα radiation (photon energy = 1253.6 eV) at a constant 50-eV pass energy. The core level binding energies were corrected with the C 1s binding energy of 284.9 eV. The C 1s, O 1s, N 1s, and Zr 3d spectra were fitted to Gaussian component peaks of equal full widths at half maximum. The position and intensity of the component peaks were optimized to give the best fit to the experimental spectrum.

The corrosion protection performance of these coatings was investigated in aqueous 3 wt % NaCl solutions with a potentiodynamic polarization technique and EIS. The potentiodynamic polarization measurements were performed as described in our previous article.[19] All the measurements were repeated at least four times, and good reproducibility of the results was observed. The potentiodynamic polarization curves were analyzed with Corr-View software from Scribner Associates (Southern Pines, NC).[20] This software performed the Tafel fitting and calculated the values of the corrosion potential (E_{corr}), corrosion current density (I_{corr}), and CR in millimeters per year.

The EIS measurements of the POT- and POTZRO-coated mild steel were carried out at the open circuit potential in aqueous 3 wt % NaCl solutions. The frequency was varied from 0.1 Hz to 20 kHz with an alternating-current excitation potential of 0.01 V. The analysis of the impedance spectra was performed by the fitting of the experimental results to equivalent circuits with Z-View software from Scribner Associates.[21] The quality of the fitting to the equivalent circuit was judged first by the χ^2 value and second by a comparison of the experimental data with the simulated data.

RESULTS AND DISCUSSION

Synthesis of the POT and POTZRO coatings

The cyclic voltammogram of the first scan recorded during the electrochemical polymerization of

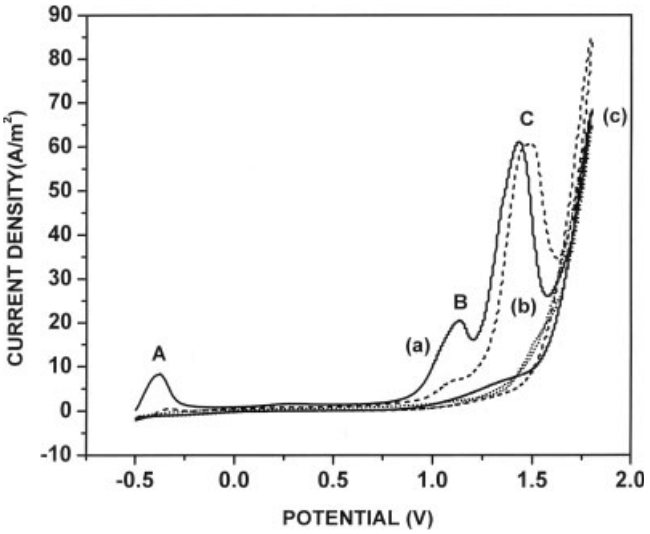

Figure 1 Cyclic voltammograms of the (a) first, (b) second, and (c) tenth scans recorded during the synthesis of a POT coating on mild steel in an aqueous tartrate solution without ZrO_2 powder.

o-toluidine on the mild steel electrode in the standard electrolyte without ZrO_2 powder is shown in Figure 1(a). The first positive cycle is characterized by anodic peaks A, B, and C at approximately −0.365, 1.137, and 1.445 V versus a saturated calomel electrode (SCE), respectively. During the reverse cycle, the anodic current density decreases rapidly, and a negligibly small current density can be observed until the end of the negative cycle. Most of the features of these cyclic voltammograms exhibit a good resemblance to those reported by Pawar et al.[19]

Anodic peak A is attributed to the formation of insoluble iron(II) tartrate ($FeC_4H_4O_6$) on the electrode surface, and as a result, the mild steel surface is passivated. Oxidation peak B at approximately 1.137 V versus SCE is attributed to the irreversible oxidation of *o*-toluidine because a black uniform film is deposited on the mild steel substrate. This suggests that the electrochemical polymerization of *o*-toluidine takes place on the mild steel electrode in an aqueous tartrate solution. Oxidation peak C at approximately 1.445 V versus SCE is assigned to the oxidation of the tartrate electrolyte.

During the second scan [Fig. 1(b)], peak A is not observed, and the current density corresponding to peak B decreases considerably. In addition, peak C is shifted in the anodic direction. This suggests that the coverage of the mild steel surface by POT inhibits the dissolution of the electrode. On repetitive cycling, voltammograms identical to that of the second scan can be obtained. However, the current density corresponding to the oxidation peaks decreases gradually with the number of scans. A visual inspection of the mild steel electrode after 10 scans reveals the formation of an adherent black POT coating. Thus, the electrochemical polymerization of *o*-toluidine on the mild steel substrate occurs in two steps from an aqueous tartrate solution.

The cyclic voltammogram of the first scan recorded during the electrochemical polymerization of *o*-toluidine on the mild steel electrode in the standard electrolyte with ZrO_2 powder is shown in Figure 2(a). This voltammogram of the first scan shows strikingly different characteristics in comparison with that recorded in the standard electrolyte without ZrO_2 nanoparticles. Indeed, anodic peak A has disappeared, and the first positive cycle indicates oxidation peaks B and C at approximately 1.189 and 1.598 V versus SCE, respectively. During the reverse cycle, the anodic current density decreases rapidly, and a negligibly small current density can be observed until the end of the negative cycle.

It may be argued that because of the common hydrophilic character of the ZrO_2 powder, these nanoparticles are easily attached to the electrode surface. Consequently, the attachment of ZrO_2 nanoparticles modifies the electrode surface before the electrochemical polymerization. The absence of anodic peak A corresponding to the dissolution of the mild steel substrate supports this argument, which indicates the stabilization of the electrode surface in the presence of ZrO_2 nanoparticles. *o*-Toluidine is readily and concurrently concentrated on the mild steel substrate in the standard electrolyte with ZrO_2 nanoparticles, and this results in a greater chance for nucleation; hence, a higher polymerization rate is observed.

Thus, the absence of anodic peak A when ZrO_2 nanoparticles are in the standard electrolyte indi-

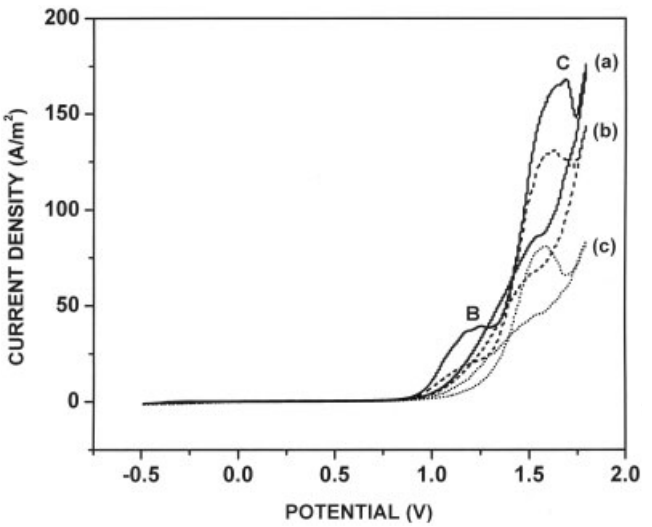

Figure 2 Cyclic voltammograms of the (a) first, (b) second, and (c) tenth scans recorded during the synthesis of a POT coating on mild steel in an aqueous tartrate solution with ZrO_2 powder.

cates that the nanoparticles affect the passivation process of the electrode surface, and subsequently, the electrochemical polymerization of *o*-toluidine on the mild steel substrate occurs in a single step from the standard electrolyte containing ZrO_2 nanoparticles.

Furthermore, the current densities corresponding to oxidation peaks B and C are significantly higher than those observed in the cyclic voltammogram recorded in the standard electrolyte without ZrO_2 nanoparticles. This suggests that the polymerization rate increases significantly with the aid of ZrO_2 nanoparticles present in the standard electrolyte. Also, the peak potentials of the oxidation peaks are observed to shift in the positive direction in the presence of ZrO_2 nanoparticles.

On repetitive cycling [Fig. 2(b)], voltammograms identical to that of the first scan can be obtained, and the current density corresponding to the oxidation peaks decreases gradually with the number of scans.

Visually, the appearance of the POTZRO coating synthesized from the standard electrolyte with ZrO_2 nanoparticles is drastically different from that of the pure POT coating. The POTZRO nanocomposite coating is shiny, more compact, and strongly adherent to the mild steel surface. The POTZRO coating adherence is enhanced when the coating is synthesized in the standard electrolyte with ZrO_2 nanoparticles. The coating adherence, estimated by standard cellotape, is approximately 100%. The coating thickness was also estimated as follows:[22]

$$d = \frac{QM}{2F\rho}$$

where Q (C) is the specific overall charge for the electrochemical polymerization, ρ is the density of POT (1.34 g/cm^3), M is the molar mass (107.15 g/mol), and F is the Faraday constant (96,500 C) The thicknesses of the POT and POTZRO coatings were found to be approximately 0.35 and 3.8 μm, respectively.

Characterization of the coatings

The FTIR spectra of POT, ZrO_2 nanoparticles, and POTZRO nanocomposite are shown in Figure 3. The main characteristic bands of POT are assigned as follows:[23–26] the broad band at approximately 3383 cm^{-1} is due to the N—H stretching mode, the band at approximately 2922 cm^{-1} is associated with C—H stretching in the methylene group, the C=N and C=C stretching modes for the quinoid and benzoid rings occur at 1600 and 1500 cm^{-1}, the bands at approximately 1310 and 1251 cm^{-1} are assigned to the C—N stretching mode for benzoid rings, the band at approximately 1118 cm^{-1} is attributed to a plane bending vibration of C—H (which is formed during protonation), and the bands between 800 and 700 cm^{-1} reveal the occurrence of the 1–3-substitutions. As can be seen in Figure 3(c), the main characteristic bands of the pure POT and ZrO_2 nanoparticles appear in the FTIR spectrum of the POTZRO

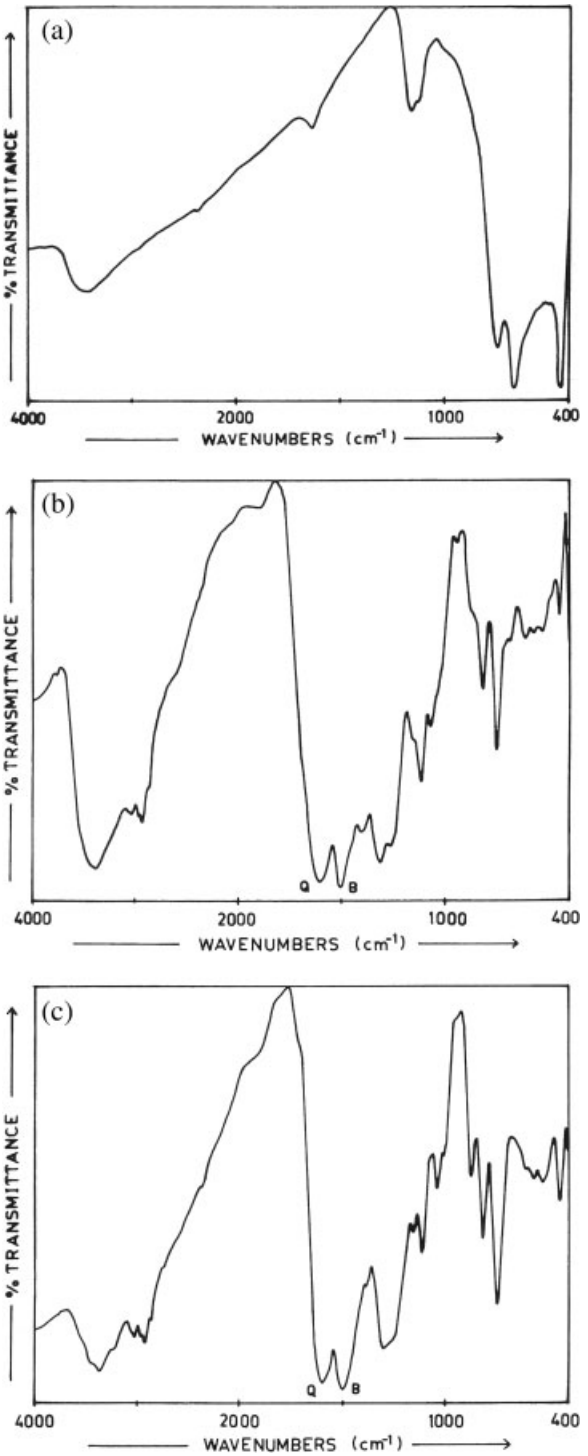

Figure 3 FTIR spectra of the (a) ZrO_2 nanoparticles, (b) pure POT, and (c) POTZRO nanocomposite.

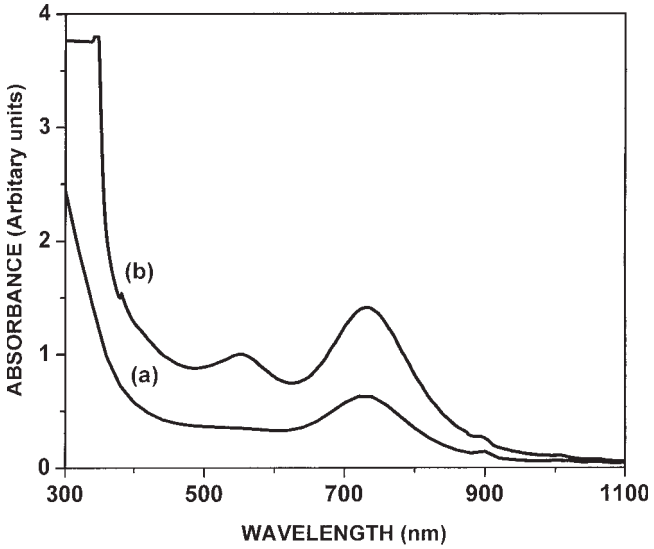

Figure 4 Optical absorption spectra of (a) POT and (b) POTZRO nanocomposite coatings synthesized on mild steel. (The spectrum was recorded *ex situ* in a dimethyl sulfoxide solution.)

nanocomposite. The bands at 1600, 1500, 1310, and 1251 cm^{-1}, corresponding to the stretching modes of C=N, C=C, and C—N, are shifted to lower wave numbers, which may be attributed to the incorporation of the ZrO_2 nanoparticles into the POT matrix. The splitting of the band at 1118 cm^{-1} that formed during the protonation into two bands at 1155 and 1113 cm^{-1} reveals that the incorporation of ZrO_2 nanoparticles has an effect on the doping of POT.

The optical absorption spectrum of the POT coating [Fig. 4(a)] shows a well-defined peak at approximately 740 nm, and it is attributed to the formation of the emeraldine salt (ES) form of POT, which is the only electrically conducting phase of POT.[27] The optical absorption spectrum of the POTZRO coating [Fig. 4(b)] exhibits a noticeable difference in comparison with Figure 4(a). First, it indicates an increase in the intensity of the peak at approximately 750 nm. Second, it shows an emergence of a peak at approximately 540 nm. The peak at approximately 540 nm is the signature of the formation of the pernigraniline base (PB) form of POT. PB is the fully oxidized form of POT and is insulating in nature.[27] The simultaneous appearance of the peaks at 750 and 540 nm clearly reveal the formation of a mixed phase of ES and PB forms of POT. The formation of the mixed phase may be attributed to the higher polymerization rate due to the presence of ZrO_2 nanoparticles in the standard electrolyte during the synthesis of the POTZRO nanocomposite coating. Thus, the optical absorption spectroscopy results are in agreement with the cyclic voltammetry.

The surface morphology of the pure POT and POTZRO nanocomposite coatings synthesized on mild steel were characterized with SEM. The surface morphology of the pure POT coating [Fig. 5(a)] is relatively rough and is characterized by the presence of the pores in the coating. The inset of Figure 5(b) shows that the surface morphology of the POTZRO nanocomposite coating on mild steel is uniform, featureless, and pore-free. There are two possible explanations for the formation of the uniform and smooth surface morphology. One possible explanation is that the ZrO_2 particles are filling the pores in the coating. Another possibility is that the presence of these particles simply changes the polymer morphology.

The energy-dispersive X-ray (EDX) analysis of the POTZRO coating was also performed to confirm the incorporation of the ZrO_2 nanoparticles into the POT matrix. As expected, the signal due to Zr can be clearly detected in the EDX spectrum, as shown in Figure 5(b), and this proves that the ZrO_2 nanoparticles are incorporated into the POT matrix. In addition, weak signals at 0.7 and 7 keV can also be observed, and this reveals the presence of Fe in the coating. It seems that the dissolution of the LCS substrate occurs during the deposition of POT, and a negligibly small amount of iron is codeposited in the conductive polymer film.

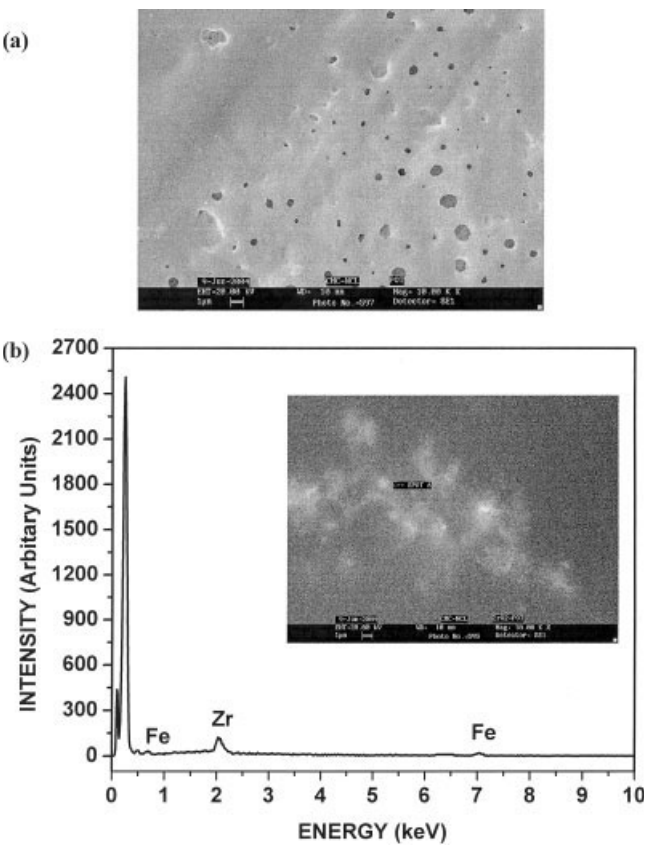

Figure 5 (a) SEM image of POT and (b) EDX spectrum of the POTZRO nanocomposite coatings synthesized on mild steel. The inset of part b shows the SEM image of a POTZRO nanocomposite coating.

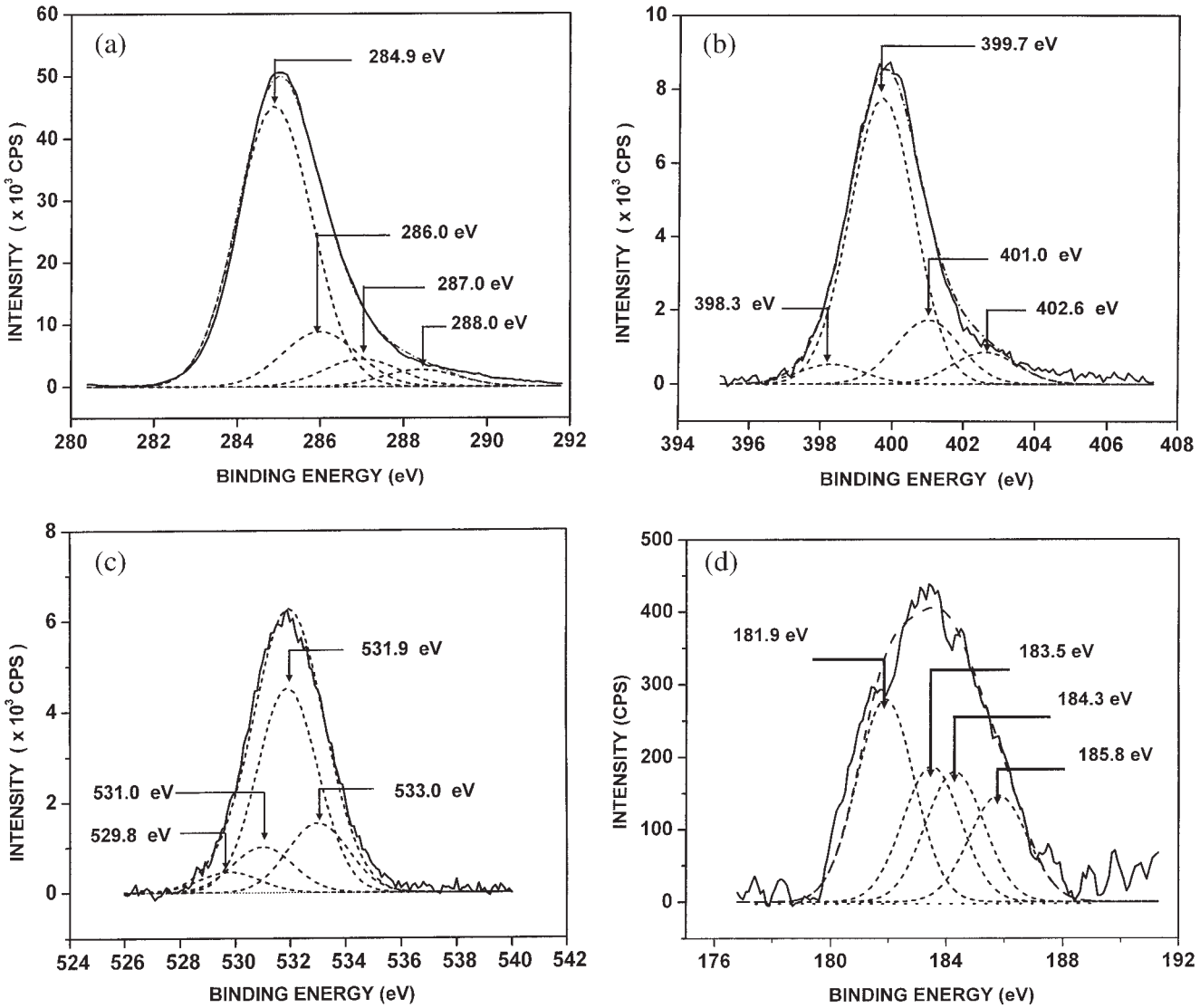

Figure 6 XPS spectra (a) C 1s, (b) N 1s, (c) O 1s, and (d) Zr 3d of a POTZRO nanocomposite coating synthesized on mild steel.

To further confirm the incorporation of the ZrO_2 nanoparticles into the POT matrix, the POTZRO nanocomposite coatings synthesized on mild steel substrates were analyzed with XPS. The XPS analysis reveals the presence of C 1s (74%), O 1s (11%), N 1s (14%), and Zr 3d (1%) in the POTZRO nanocomposite coating. The deconvoluted spectra of C 1s, O 1s, N 1s, and Zr 3d are shown in Figure 6.

The C 1s spectrum has been deconvoluted into four components at 284.9, 286, 287, and 288.4 eV [Fig. 6(a)] with relative areas of 1 : 0.19 : 0.09 : 0.07, respectively. The main peak at 284.9 eV is attributed to the C—C bond in the benzene ring of POT. The peaks at 286 and 287 eV are assigned to the presence of C—N and C=N bands, respectively. The peak at 288.4 eV is attributed to the carboxylic acid type carbons and indicates the presence of tartrate anions as doping ions in the POT coating.

The deconvoluted N 1s spectrum of the POTZRO nanocomposite coating is shown in Figure 6(b). This spectrum has been deconvoluted into four components at 398.3, 399.7, 401.0, and 402.6 eV with the relative areas of 0.07 : 1 : 0.23 : 0.11, respectively. These components reveal the presence of quinoid imine (=N—), benzoid amine (—NH—), and positively charged nitrogen atoms. The peak at 398.3 eV is attributed to the =N— imine nitrogen. The peak at 399.7 eV is due to the amine nitrogen. The peaks at 401.0 and 402.6 eV are attributed to positively charged nitrogen and correlated with the doping level of the POT coating. The doping level of the POTZRO coating has been calculated from the area ratio of the positively charged nitrogen signal to the total N 1s signal to be approximately 24%.

The deconvoluted O 1s spectrum of the POTZRO nanocomposite coating is shown in Figure 6(c). The

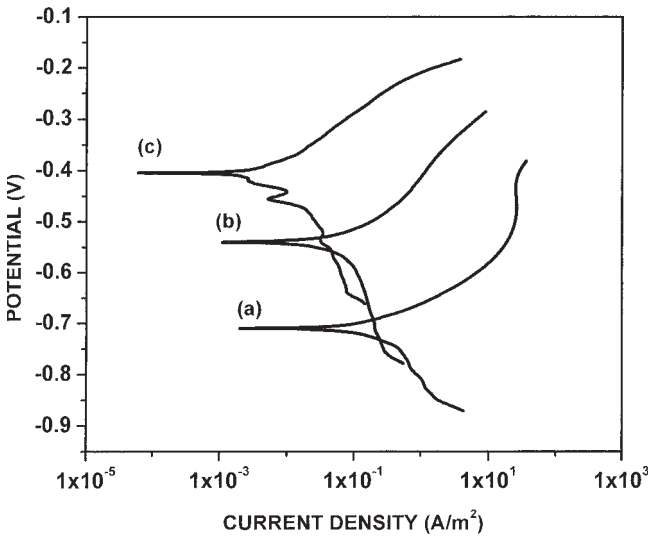

Figure 7 Potentiodynamic polarization curves for (a) uncoated mild steel, (b) POT-coated mild steel, and (c) POTZRO-coated mild steel recorded in aqueous 3 wt % NaCl solutions.

O 1s spectrum has been deconvoluted into four peaks at 529.8, 531.0, 532.0, and 533.0 eV with the relative areas of 0.1 : 0.23 : 0.33 : 1.0, respectively. The peak at 529.8 eV is attributed to the oxygen atoms of the ZrO_2. The presence of the peak at 531.0 eV is due to the oxygen originating from surface water contamination. Matsuoka et al.[28] attributed this peak to oxygen possibly bound to Zr. The presence of the peaks at 532.0 and 533.0 eV is attributed to C=O and O=C—O^- and indicates the incorporation of tartrate anions as dopants into the coating.

The deconvoluted Zr 3d spectrum of the POTZRO nanocomposite coating is shown in Figure 6(d). The Zr 3d spectrum has been deconvoluted into four peaks at binding energies of 181.9, 184.3, 183.5, and 185.8 eV. It seems that there are two types of ZrO_2 present on the metal surface. Peaks Zr $3d_{5/2}$ and Zr $3d_{3/2}$, observed at 181.9 and 184.3 eV, are attributed to the first type of ZrO_2 nanoparticle sitting in the POT matrix.[28,29] The spin orbit splitting between the other two peaks observed at 183.5 and 185.8 eV is approximately 2.3 eV, and their area ratio is approximately 1.3. This suggests that these peaks also correspond to Zr $3d_{5/2}$ and Zr $3d_{3/2}$, respectively. However, these peaks indicate the shift in the binding energies versus the characteristic Zr 3d peaks in ZrO_2. Therefore, these peaks may possibly be attributed to the second type of ZrO_2 nanoparticle adsorbed on the metal surface. The observed shift in the binding energy in the characteristic peaks may be attributed to the electric field at the mild steel surface. Thus, the XPS results reveal that the ZrO_2 nanoparticles are incorporated into the POT matrix. The O/Zr area ratio originating from ZrO_2 is approximately 2, a value that corresponds to the stoichiometry of ZrO_2. The atomic concentration of ZrO_2 on the surface of the POTZRO coatings synthesized on mild steel in the standard electrolyte containing 1.25 g/L ZrO_2 powder has been estimated with the XPS data to be 0.16%.

Evaluation of the corrosion protection performance

The coating porosity is one of the important parameters that strongly govern the anticorrosive behavior of coatings. The porosity of pure POT and POTZRO coatings on mild steel substrates was determined from potentiodynamic polarization measurements. The potentiodynamic polarization curves recorded for uncoated mild steel, POT-coated mild steel, and POTZRO-coated mild steel in aqueous 3 wt % NaCl are shown in Figure 7. The values of E_{corr}, I_{corr}, the Tafel constants (β_a and β_c), the polarization resistance (R_p), and CR obtained from these curves are given in Table I. The porosity of the coating was calculated as follows:[30]

$$P = \frac{R_{ps}}{R_{pc}} 10^{-\left(\frac{|\Delta E_{corr}|}{\beta_a}\right)}$$

where P is the total porosity, R_{ps} (Ω) is the polarization resistance of the uncoated mild steel, R_{pc} (Ω) is the measured polarization resistance of the coated mild steel, ΔE_{corr} is the difference between the corrosion potentials (V), and β_a (V/dec) is the anodic Tafel slope for the uncoated mild steel substrate. The porosity of the POT and POTZRO coatings was found to be approximately 0.16 and 4.11×10^{-4} %. The lower value of the porosity in the POTZRO nanocomposite coating provides an improvement in the corrosion resistance by hindering the access of the electrolyte to the mild steel substrates.

The potentiodynamic polarization curve for POT-coated mild steel is shown in Figure 7(b). I_{corr}

TABLE I
Potentiodynamic R_p Measurement Results

Sample	E_{corr} (V)	I_{corr} (A/m^2)	β_a (V/dec)	β_c (V/dec)	R_p (Ω/m^2)	CR (mm/year)	P (%)
Uncoated mild steel	−0.710	0.3071	0.084	0.185	816.82	0.35	–
POT coated on mild steel	−0.538	0.08523	0.109	0.406	4,386.28	0.09	0.16
POTZRO nanocomposite coated on mild steel	−0.398	0.000691	0.094	0.175	38,393.00	0.007	0.0004

decreases from 0.3071 A/m^2 for uncoated mild steel to 0.08523 A/m^2 for POT-coated mild steel. E_{corr} increases from −0.710 V versus SCE for uncoated mild steel to −0.538 V versus SCE for POT-coated mild steel. The positive shift of 0.172 V versus SCE in E_{corr} indicates the protection of the mild steel surface by the POT coating. The CR of mild steel is reduced as a result of the reduction in I_{corr}. The CR of mild steel is approximately 0.09 mm/year, which is approximately 4 times lower than that observed for uncoated mild steel.

The potentiodynamic polarization curve for POTZRO-nanocomposite-coated mild steel recorded in an aqueous 3 wt % NaCl solution is shown in Figure 7(c). The E_{corr} value increases from −0.710 V versus SCE for uncoated mild steel to −0.398 V versus SCE for POTZRO-coated mild steel. The positive shift of 0.312 V versus SCE in E_{corr} indicates the protection of the mild steel surface by the POTZRO coating. Furthermore, the I_{corr} value for POTZRO-coated mild steel is far lower than the corresponding values for uncoated mild steel and for POT-coated mild steel, indicating the corrosion-resistant feature of the POTZRO nanocomposite coating. I_{corr} decreases from 0.3071 A/m^2 for uncoated mild steel to 0.0069 A/m^2 for POTZRO-nanocomposite-coated mild steel. The CR of POTZRO-coated mild steel is approximately 0.007 mm/year. Thus, the incorporation of ZrO_2 into the POT matrix lowers the CR of the mild steel by approximately 51 times, and this is attributed to the low porosity of the POTZRO nanocomposite coating due to the filling of the pores by ZrO_2 nanoparticles. These results reveal the capability of the POTZRO nanocomposite to act as a protective layer on mild steel. The protection efficiency (PE) of the coating was calculated as follows:

$$PE(\%) = \left[\frac{R_{pc} - R_{ps}}{R_{pc}}\right] \times 100$$

The PE values of POT and POTZRO nanocomposite coatings calculated from potentiodynamic polarization data are approximately 81 and 98%, respectively. This implies that the POTZRO nanocomposite coating provides better protection than POT.

Nyquist impedance plots of uncoated mild steel, POT-coated mild steel, and POTZRO-coated mild steel in aqueous 3 wt % NaCl are shown in Figure 8. These impedance plots were modeled by the equivalent circuit depicted in the inset of Figure 8(a). The equivalent circuit consists of the electrolyte resistance (R_s), pore resistance (R_p), coating capacitance (C_c), charge-transfer resistance (R_{ct}), and double-layer capacitance (C_{dl}). Instead of capacitance, a constant phase element (CPE) was used. The CPE represents the deviation from the true capacitance behavior. The quality of the fitting to the equivalent circuit

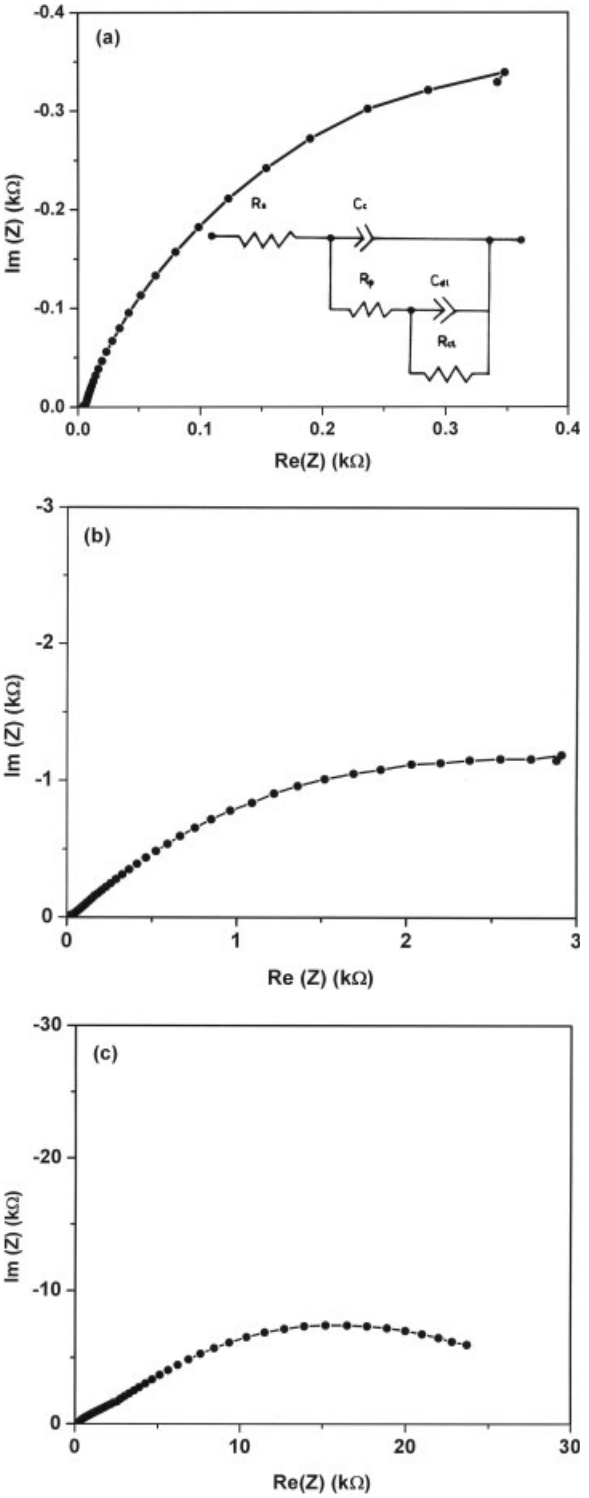

Figure 8 Nyquist impedance plots for (a) uncoated mild steel, (b) POT-coated mild steel, and (c) POTZRO-coated mild steel synthesized with cyclic voltammetry. The plots were recorded at an open circuit potential in aqueous solutions of 3 wt % NaCl. The inset of part a shows the equivalent circuit used for modeling the impedance plots.

was judged first by the χ^2 value (i.e., the sum of the square of the differences between theoretical and experimental points) and second by the limitation of

TABLE II
Impedance Parameter Values Extracted from the Fit to the Equivalent Circuit for the Impedance Spectra Recorded in an Aqueous 3 wt % NaCl Solution

Sample	R_s (Ω)	R_p (Ω)	C_c (F/m)	n	R_{ct} (Ω)	C_{dl} (F/m)	n	PE (%)
Uncoated mild steel	4.93	21.00	2.0688×10^{-3}	0.80	1,041	9.8753×10^{-5}	0.90	–
POT coated on mild steel	10.84	24.56	2.9463×10^{-6}	0.80	4,978	1.8906×10^{-4}	0.60	80
POTZRO nanocomposite coated on mild steel	178.3	1625	1.7367×10^{-6}	0.60	35,582	1.9635×10^{-5}	0.70	97

the relative error in the value of each element in the equivalent circuit to 5%. The χ^2 values for the fitting of the impedance plots were observed to be approximately 10^{-4}, and the error bars are not visible in Figure 8.

The impedance plot of uncoated mild steel [Fig. 8(a)] can be fitted with two semicircles, a smaller one at a high frequency range followed by a larger one at lower frequencies. The first semicircle is attributed to the formation of the corrosion film, and the second one is attributed to processes occurring underneath the corrosion film. Thus, the impedance plot of uncoated mild steel is characteristic of a system undergoing dissolution with the precipitation of a corrosion film at the electrode surface.

The impedance plot of POT-coated mild steel [Fig. 8(b)] was modeled with the same equivalent circuit depicted in the inset of Figure 8(a). However, the parameter values of the best fit to the impedance plot are significantly different than those obtained for uncoated mild steel. In this case, the first capacitive loop is attributed to the POT coating itself, and the second one is attributed to processes occurring underneath the coating. Table II gives the values for the representative impedance parameters of the best fit to the experimental data using the circuit shown in the inset of Figure 8(a) for uncoated mild steel, POT-coated mild steel, and POTZRO-coated mild steel.

PE was calculated with the following expression:

$$PE(\%) = \left[\frac{R_{ctp} - R_{ct}}{R_{ctp}}\right] \times 100$$

where R_{ct} (Ω) and R_{ctp} (Ω) denote the charge-transfer resistance of mild steel without and with a coating, respectively. The PE calculated from EIS data is approximately 80%. This is in agreement with the potentiodynamic polarization results.

The impedance plot of POTZRO coated on mild steel is shown in Figure 8(c). The values of the impedance parameters obtained by the modeling of the experimental impedance plot with the equivalent circuit depicted in the inset of Figure 8(a) are given in Table II. The higher values of R_{ct} and R_p and lower values of C_c and C_{dl} indicate that the POTZRO nanocomposite coating offers better corrosion performance to mild steel. The PE calculated from EIS data is approximately 97%, which is in agreement with the polarization result.

CONCLUSIONS

POTZRO nanocomposite coatings have been synthesized electrochemically on mild steel in ZrO_2-containing aqueous solutions. The characterization of the nanocomposite coatings reveals that the ZrO_2 nanoparticles are successfully incorporated into the POT matrix. The electrochemical polymerization of *o*-toluidine on mild steel occurs in a single step in a ZrO_2-containing aqueous solution. The surface morphology of the nanocomposite coating is uniform and more compact. A potentiodynamic polarization and EIS study shows that the incorporation of ZrO_2 nanoparticles significantly improves the corrosion protection properties of the POT coating. This study indicates that the POTZRO nanocomposite coating provides better corrosion protection than POT and can be considered a potential coating material to protect steel against corrosion in aqueous 3 wt % NaCl.

References

1. Handbook of Conducting Polymers; Skotheim, T. A., Ed.; Marcel Dekker: New York, 1986; Vols. I and II.
2. Nalwa, H. S. Handbook of Organic Conductive Molecules and Polymers; Wiley: New York, 1997; Vols. 1–4.
3. Salaneck, W. R.; Clark, D. T.; Samuelsen, E. J. Science and Applications of Conducting Polymers; Adam Hilger: Bristol, PA, 1991.
4. Aldissi, M. Intrinsically Conducting Polymers: An Emerging Technology; Kluwer Academic: Dordrecht, 1993.
5. Chandrasekhar, P. Conducting Polymers: Fundamentals and Applications; Kluwer Academic: Dordrecht, 1999.
6. Bereket, G.; Hur, E.; Sahin, Y. Prog Org Coat 2005, 54, 63.
7. Zhang, T.; Zeng, C. L. Electrochim Acta 2005, 50, 4721.
8. Popovic, M. M.; Grgur, B. N. Synth Met 2004, 143, 191.
9. Ogurtsov, N. A.; Pud, A. A.; Kamarchik, P.; Shapoval, G. S. Synth Met 2004, 143, 43.
10. Shinde, V.; Sainkar, S. R.; Patil, P. P. J Appl Polym Sci 2005, 96, 685.
11. Shinde, V.; Sainkar, S. R.; Patil, P. P. Corros Sci 2005, 47, 1352.
12. Yada, S.; Hasegawa, A.; Suda, H.; Uchimaru, Y.; Haraya, K.; Tsuji, T.; Otake, K. Chem Mater 2004, 16, 2363.
13. Hasik, M.; Wenda, E.; Bernasik, A.; Kowalski, K.; Sobczak, J. W.; Sobezak, E.; Bielanska, E. Polymer 2003, 44, 7809.

14. Kinyanjui, J. M.; Hatchett, D. W.; Smith, J. A.; Josowicz, M. Chem Mater 2004, 16, 3390.
15. Ma, Z. A.; Tan, K. L.; Kang, E. T. Synth Met 2000, 114, 17.
16. Kawai, K.; Mihara, N.; Kuwataba, S.; Yoneyama, H. J Electrochem Soc 1990, 137, 1793.
17. Kuwataba, S.; Kishimoto, A.; Tanaka, T.; Yoneyama, H. J Electrochem Soc 1994, 141, 10.
18. Ferreira, C. A.; Domenech, S. C.; Lacaze, P. C. J Appl Electrochem 2001, 31, 49.
19. Pawar, P.; Sainkar, S. R.; Patil, P. P. J Appl Polym Sci 2007, 103, 1868.
20. Electrochemical Corrosion Software—CorrWare and CorrView; Scribner Associates: Southern Pines, NC.
21. Electrochemical Impedance Software—Z-Plot and Z-View; Scribner Associates: Southern Pines, NC.
22. Tuken, T.; Yazici, B.; Erbil, M. Prog Org Coat 2005, 54, 372.
23. Tang, J.; Jing, X.; Wang, B.; Wang, F. Synth Met 1988, 24, 231.
24. Ohsaka, T.; Ohnuki, Y.; Oyama, N.; Katagiri, G.; Kamisako, K. J Electroanal Chem 1984, 161, 399.
25. Zheng, W. Y.; Levon, K.; Taka, T.; Laakso, J.; Osterholm, J. E. Polym J 1996, 28, 412.
26. Neoh, K. G.; Kang, E. T.; Tan, K. L. J Phys Chem 1991, 95, 10151.
27. Patil, S. Ph.D. Thesis, North Maharashtra University, 2000.
28. Matsuoka, M.; Isotani, S.; Chubaci, J. F. D.; Miyake, S.; Setsuhara, Y.; Ogata, K.; Kuratani, N. J Appl Phys 1996, 80, 1177.
29. Yu, G. Q.; Tay, B. K.; Zhao, Z. W. Appl Phys A 2005, 81, 405.
30. Creus, J.; Mazille, H.; Idrissi, H. Surf Coat Technol 2000, 130, 224.